

PARTICLE SMOOTHING FOR SOLVING AMBIGUITY PROBLEMS IN ONE-SHOT STRUCTURED LIGHT SYSTEMS

F. van der Heijden, F. F. Berendsen, L. J. Spreeuwiers and E. Schippers

Signals and Systems Group, Faculty of EEMCS, University of Twente, P.O.Box 217, 7500 AE Enschede, The Netherlands

Keywords: 3D Depth reconstruction, One-shot structured light system, Particle filtering, Jump Markov linear systems.

Abstract: One-shot structured light systems for 3D depth reconstruction often use a periodic illumination pattern. Finding corresponding points in the image and projector plane, needed for a triangulation, boils down to phase estimation. The $2\pi N$ ambiguities in the phase cause ambiguities in the reconstructed depth. This paper solves these ambiguities by constraining the solution space to scenes that only contain objects with flat surfaces, i.e. polyhedrons. We develop a new particle filter that estimates the depth and solves the ambiguity problem. A state model is proposed for piecewise continuous signals. This state model is worked out to find the optimal proposal density of the particle filter. The approach is validated with a demonstration.

1 INTRODUCTION

We consider the problem of 3D object surface reconstruction based on a sinusoidally modulated illumination pattern. Figure 1 shows an example. Depth information of the surface is obtained from the phase of the pattern observed by a camera. This is the principle of phase-measuring profilometry (Su and Chen, 2001). Sinusoidal patterns are beneficial because the phase can be estimated easily and accurately, provided that the period of the signal is small. This all can be done with a single shot of the scene, thus allowing moving objects. Since the phase of a sine has an ambiguity of multiples of 2π , the depth derived from the phase is also ambiguous. If the range of depths is limited to a 2π -zone, or if the depth is a smooth function without jumps, the ambiguity is easily bypassed. Otherwise, more involved methods must be applied. For that, two principles are available. One possibility is to augment the pattern such that more information becomes available (Su and Chen, 2001). The other possibility is to constrain the solution space. In this paper we focus on this second possibility. We only consider objects, that are made up by flat surfaces, i.e. polyhedrons. Amongst all possible solutions we have to select the one that describes flat surfaces. With a suitable geometrical set-up of the camera and the projector, this particular solution can be made unique (van der Heijden et al., 2009).

The question is how to find this unique solution. We address this problem by scanning the image in

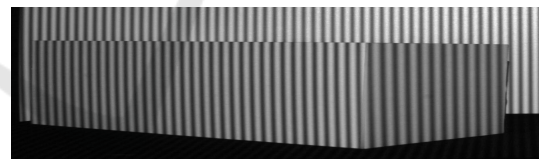


Figure 1: Sinusoidal illumination.

the phase direction along rows in the camera plane. We use the row co-ordinate, denoted by ξ , as the running variable. Each row of the image is a mapping from a 2D slice $[X(\xi) Y(\xi) Z(\xi)]$ of the 3D surface of the scene. Suppose that we have found the depth co-ordinate $Z(\xi)$. Then, using the pinhole geometry of the camera, it is easy to find $X(\xi)$ and $Y(\xi)$. So, we only need to concentrate on finding $Z(\xi)$. For simplicity, and without loss of generality, we ignore the Y -co-ordinate, so that we have a 2D geometry, i.e. $[X(\xi) Z(\xi)]$.

Since the scene is made up by multiple objects, the depth $Z(\xi)$ contains step transitions. Between two successive transitions, $[X(\xi) Z(\xi)]$ form a linear segment due to the assumption of having flat surfaces. Each linear segment can be represented by two parameters, e.g. the slope and the interception of the depth. We model this piecewise linear behavior of the depth with a system state equation for $Z(\xi)$. The state equation does not contain process noise except for the step transitions that occur randomly. We estimate the positions of the transitions as well as the two parameters of each segment with a new particle filter.

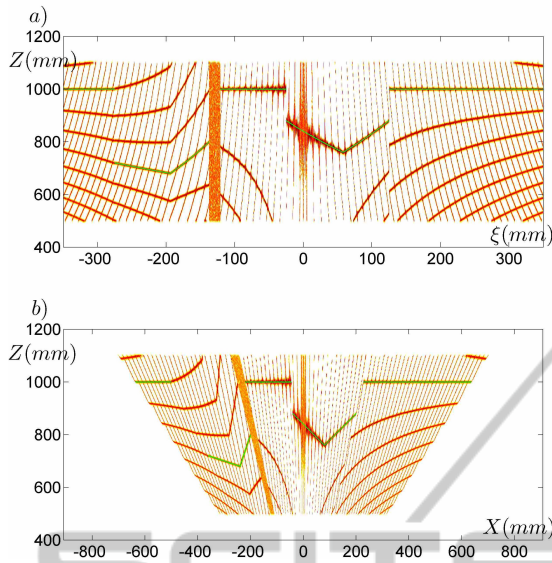


Figure 4: Ambiguous solutions in a) the Z, ξ domain, and b) in the Z, X domain. The green lines form the ground truth.

whereas the thin almost vertical solutions are due to $\sin(\phi) = \sin(\pi - \phi + 2n\pi)$. The green lines in the figures are the ground truth. The various trajectories in the X, Z domain are all slightly curved, except for one: the true solution. We also note in figure 4 that the ambiguity near the optical axis of the projector diminishes. This is at the cost of an increasing noise sensitivity. The figure also shows a cone where all X, Z are evenly likely. This area corresponds to a part in the scene that is not illuminated because of occlusion.

3 MODELING THE SYSTEM

Starting with the definition of the state vector, this section introduces a suitable state equation. The state vector that we consider consists of two continuous states Z_k, a_k , and one Boolean state r_k . Here Z_k is the depth at a position ξ_k , and a_k is the slope of the surface, i.e. $a_k = \partial Z_k / \partial X_k$. We combine Z_k and a_k in a 2D vector: $\mathbf{x}_k = [Z_k \ a_k]^T$. The variable r_k indicates that a jump transition has taken place at position k . The two possible outcomes are J and S , i.e. "jump" and "smooth", respectively. The probability of a jump equals P_J . We assume that the variable r_k is memoryless. That is: $\Pr(r_k | r_{0:k-1}, \mathbf{x}_{0:k-1}) = \Pr(r_k)$. If $r_k = J$, the vector \mathbf{x}_k is reset to a new, random state, drawn from a bivariate uniform distribution:

$$\begin{aligned} p(\mathbf{x}_k | r_k = J, r_{0:k-1}, \mathbf{x}_{0:k-1}) &= p(\mathbf{x}_k | r_k = J) \\ &= U(Z_k, I_Z) U(a_k, I_a) \end{aligned} \quad (4)$$

$U(Z_k, I_Z)$ denotes a uniform distribution of Z_k within an interval I_Z .

If no jump takes place, i.e. $r_k = S$, then \mathbf{x}_k proceeds continuously. From the pinhole equation $X = Z\xi/D_C$ and the definition of the slope $a_k = \partial Z / \partial X$ it is easy to derive that $\partial Z / \partial \xi = aZ / (D_C - a\xi)$. From this, we obtain the following nonlinear system state equation $\mathbf{f}_k(\mathbf{x}_k)$:

$$\mathbf{x}_{k+1} = \begin{bmatrix} Z_{k+1} \\ a_{k+1} \end{bmatrix} = \mathbf{f}_k(\mathbf{x}_k) = \begin{bmatrix} Z_k \frac{D_C - a\xi_k}{D_C - a\xi_{k+1}} \\ a_k \end{bmatrix} \quad (5)$$

Since there is no process noise:

$$p(\mathbf{x}_k | r_k = S, r_{0:k-1}, \mathbf{x}_{0:k-1}) = \delta(\mathbf{x}_k - \mathbf{f}_k(\mathbf{x}_{k-1})) \quad (6)$$

Within a continuity interval, \mathbf{x}_k proceeds deterministically. Estimation of this part of a trajectory boils down to estimation of two parameters, e.g. the interception and the slope. Recurrent estimation of these parameters can easily be accomplished by an extended Kalman filter, provided that no jumps occur, and that the measurements are unambiguous. These two conditions are not met in the present case.

4 THE PARTICLE FILTER

Our approach is inspired on algorithms for jump Markov linear systems as proposed in (Doucet et al., 2001). The most important difference between the model, discussed there, is that, conditioned on $r_{1:k}$, their system is Gaussian-linear, whereas our system is not. If in (Doucet et al., 2001) the sequence $r_{1:k}$ is given, the corresponding sequence $\mathbf{x}_{1:k}$ is Gaussian. In our case, it is still multimodal. Especially, when a jump occurs, \mathbf{x}_k is first uniform instead of Gaussian, and after one measurement it becomes multi-modal. We are able to solve the ambiguity because, after a jump, the correct trajectory is constraint.

We adapted the algorithm in (Doucet et al., 2001) as follows. We augment each particle $r_{1:k}^{(i)}$ by two statistics: $\mathbf{m}_{k|k}^{(i)}$ and $\mathbf{P}_{k|k}^{(i)}$. These are the posterior mean of \mathbf{x}_k and the corresponding error covariance matrix, respectively. The connotation is as follows. Suppose that the last jump in the sequence $r_{0:k}^{(i)}$ has taken place at position $k_j < k$. At that position, a new sample $\mathbf{x}_{k_j}^{(i)}$ is drawn from $U(Z_k, I_Z) U(a_k, I_a)$. From that point on, $\mathbf{x}_k^{(i)}$ proceeds without jumps. Therefore, we can estimate \mathbf{x}_k using an extended Kalman filter yielding the statistics $\mathbf{m}_{k|k}^{(i)}$ and $\mathbf{P}_{k|k}^{(i)}$.

We only need to work out the proposal density and the weight function to establish the al-

gorithm. The optimal proposal density (Arulampalam et al., 2002) and (Doucet et al., 2001), is $p(r_k, \mathbf{x}_k | r_{0:k-1}^{(i)}, \mathbf{x}_{0:k-1}^{(i)}, y_k)$. This is the density from which we draw new samples. We write:

$$p(r_k, \mathbf{x}_k | r_{0:k-1}^{(i)}, \mathbf{x}_{0:k-1}^{(i)}, y_k) = p(\mathbf{x}_k | r_k, \mathbf{x}_{0:k-1}^{(i)}, y_k) \Pr(r_k | \mathbf{x}_{0:k-1}^{(i)}, y_k) \quad (7)$$

This shows that we first can draw a sample of r_k , and conditioned on that, a sample for \mathbf{x}_k . We concentrate on r_k first.

The first step is to expand $\Pr(r_k | \mathbf{x}_{0:k-1}^{(i)}, y_k)$ using Bayes' theorem:

$$\Pr(r_k = J | \mathbf{x}_{0:k-1}^{(i)}, y_k) = \frac{P_J p(y_k | r_k = J, \mathbf{x}_{k-1}^{(i)})}{(1 - P_J) p(y_k | r_k = S, \mathbf{x}_{k-1}^{(i)}) + P_J p(y_k | r_k = J, \mathbf{x}_{k-1}^{(i)})} \quad (8)$$

The density with $r_k = J$ in this expression follows from eq. 3 and 4:

$$\begin{aligned} p(y_k | r_k = J, \mathbf{x}_{k-1}^{(i)}) &= p(y_k | r_k = J) \\ &= \int_{-\infty}^{+\infty} p(y_k, Z_k) dZ_k \\ &= \int_{-\infty}^{+\infty} p(Z_k | y_k) p(Z_k) dZ_k \\ &= \int_{-\infty}^{+\infty} N(y_k, h_k(Z_k), \sigma_v^2) U(Z_k, I_Z) dZ_k \end{aligned} \quad (9)$$

The density in eq. 8 with $r_k = S$ follows from eq. 3 and 6:

$$p(y_k | r_k = S, \mathbf{x}_{k-1}^{(i)}) = N(y_k, h_k(\mathbf{f}_k(\mathbf{x}_{k-1}^{(i)})), \sigma_v^2) \quad (10)$$

Substitution of eq. 9 and 10 in eq. 8 yields:

$$\Pr(r_k = J | \mathbf{x}_{0:k-1}^{(i)}, y_k) = \left(1 + \frac{(1 - P_J) N(y_k, h_k(\mathbf{f}_k(\mathbf{x}_{k-1}^{(i)})), \sigma_v^2)}{P_J \int_{-\infty}^{+\infty} N(y_k, h_k(Z_k), \sigma_v^2) U(Z_k, I_Z) dZ_k} \right)^{-1} \quad (11)$$

The result is quite intuitive. The fraction contains the likelihood ratio under the two hypotheses $r_k = S$ and $r_k = J$, respectively. If the likelihood ratio is one, the posterior probability equals the prior probability. If the observed measurement matches the predicted measurement, the likelihood ratio will be greater than one, and as a result the posterior probability of a transition decreases.

Once a sample of r_k has been drawn, we concentrate on \mathbf{x}_k . If we have drawn $r_k^{(i)} = J$, the particle jumps, and $\mathbf{x}_k^{(i)}$ must be reset to a new, random state. The distribution to drawn from is:

$$p(\mathbf{x}_k | r_k = J, \mathbf{x}_{0:k-1}^{(i)}, y_k) = \frac{1}{\|C\|} N(y_k, h_k(Z_k), \sigma_v^2) U(Z_k, I_Z) U(a_k, I_a) \quad (12)$$

$\|C\|$ is a normalizing constant. The sample is the start of a new smooth trajectory. We initiate the statistics of that trajectory to $\mathbf{m}_{k|k} = \mathbf{x}_k^{(i)}$, and $\mathbf{P}_{k|k} = \text{diag}(\sigma_Z^2, \sigma_a^2)$. We set $\sigma_Z^2 = \sigma_v^2 / H^2(Z_k^{(i)})$ with $H(\cdot)$ the derivative of $h_k(Z_k)$. The variance of a_k is set to 16 which covers a wide band of slopes.

If we have drawn $r_k^{(i)} = S$, the density $p(\mathbf{x}_k | r_k = S, \mathbf{x}_{0:k-1}^{(i)}, y_k)$ follows from an extended Kalman update:

$$\begin{aligned} \mathbf{m}_{k|k-1}^{(i)} &= \mathbf{f}_k(\mathbf{m}_{k-1|k-1}^{(i)}) \\ S &= H_i \mathbf{F}_i \mathbf{P}_{k-1|k-1}^{(i)} \mathbf{F}_i^T H_i + \sigma_v^2 \\ \mathbf{K} &= \mathbf{F}_i \mathbf{P}_{k-1|k-1}^{(i)} \mathbf{F}_i^T H_i S^{-1} \\ \mathbf{m}_{k|k}^{(i)} &= \mathbf{m}_{k|k-1}^{(i)} + \mathbf{K} (y_k - h_k(\mathbf{m}_{k|k-1}^{(i)})) \\ \mathbf{P}_{k|k}^{(i)} &= \mathbf{F}_i \mathbf{P}_{k-1|k-1}^{(i)} \mathbf{F}_i^T - \mathbf{K} S \mathbf{K}^T \end{aligned} \quad (13)$$

\mathbf{F}_i is the Jacobian matrix of $\mathbf{f}_{k-1}(\cdot)$ evaluated at $\mathbf{m}_{k-1|k-1}^{(i)}$. H_i is the derivative of $h_k(\cdot)$ at $\mathbf{m}_{k|k-1}^{(i)}$.

Beside a proposal density to draw samples from, we also need a function to weight these samples. The weight function that corresponds to the optimal proposal density is $w_k^i = p(y_k | \mathbf{x}_k^{(i)})$. See (Arulampalam et al., 2002).

$$\begin{aligned} w_k^i &= \sum_{r_k} \int_{-\infty}^{+\infty} p(y_k | \mathbf{x}_k) p(\mathbf{x}_k | r_k, \mathbf{x}_{k-1}^{(i)}) Pr(r_k) d\mathbf{x}_k \\ &= P_J \int_{-\infty}^{+\infty} N(y_k, h_k(Z_k), \sigma_v^2) U(Z_k, I_Z) dZ_k \\ &\quad + (1 - P_J) N(y_k, h_k(\mathbf{f}_k(\mathbf{x}_{k-1}^{(i)})), \sigma_v^2) \end{aligned} \quad (14)$$

This equation works out differently for samples with a jump and samples without. If the jump samples are enumerated by i_J and the other by i_S , we find:

$$\begin{aligned} w_k^{i_J} &= P_J \int_{-\infty}^{+\infty} N(y_k, h_k(Z_k), \sigma_v^2) U(Z_k, I_Z) dZ_k \\ w_k^{i_S} &= (1 - P_J) N(y_k, h_k(\mathbf{m}_{k|k}^{(i_S)}), \sigma_v^2) \end{aligned} \quad (15)$$

A cycle of the particle filter follows the following code:

For the whole sample set $i = 1, \dots, N$:

- Sample $r_k^{(i)}$ from the distribution given in eq. 11.
- If $r_k^{(i)}$ is a jump: sample $\mathbf{x}_k^{(i_J)}$ from the distribution given in eq.12. Initiate $\mathbf{m}_{k|k}^{(i_J)}$ and $\mathbf{P}_{k|k}^{(i_J)}$ accordingly.

- If $r_k^{(i)}$ is smooth: update $\mathbf{m}_{k|k}^{(is)}$ and $\mathbf{P}_{k|k}^{(is)}$. See eq 13.
- Evaluate the weights w_k^i according to eq. 15.
- Normalize the weights $w_k^i \leftarrow w_k^i / \sum_i (w_k^i)$.
- Resample to obtain unweighed particles.

The set $\{r_k^{(i)}, \mathbf{m}_{k|k}^{(i)}\}$, $i = 1, 2, \dots$ provides us with a particle estimate of $p(r_k, \mathbf{x}_k | y_{1:k})$.

5 PARTICLE SMOOTHING

The particle filter runs in a left-to-right scanning mode. Since the filter is causal, the depth $Z(\xi)$ is estimated without using measurement data that is on the right of ξ . The transient behavior after each transition can be improved further by application of a particle smoother. After running in the forward (left-to-right) direction, a backward run clears away the remaining ambiguities near the transitions. The backward smoother, presented in (Fong et al., 2002), modifies the weights w_k^i of the particle filter according to

$$w_{k|k+1}^i = \frac{w_k^i p(r_{k+1}, \mathbf{x}_{k+1} | r_k^{(i)}, \mathbf{x}_k^{(i)})}{\sum_j w_k^j p(r_{k+1}, \mathbf{x}_{k+1} | r_k^{(j)}, \mathbf{x}_k^{(j)})} \quad (16)$$

In our case, the transition probability is given by:

$$p\left(r_k, \mathbf{x}_k | r_{k-1}^{(i)}, \mathbf{x}_{k-1}^{(i)}\right) = \begin{cases} U(\mathbf{x}_k, (I_Z \times I_a)) P_J & \text{if } r_k = J \\ \delta(\mathbf{x}_k - \mathbf{f}_{k-1}(\mathbf{x}_{k-1}^{(i)})) (1 - P_J) & \text{if } r_k = S \end{cases} \quad (17)$$

To prevent numerical instabilities, we replaced the Dirac function by a peaked Gaussian.

The backward smoother is performed as follows (input is the weighed particle representation $w_{1:K}^i$ and $(r_{1:K}^{(i)}, \mathbf{x}_{1:K}^{(i)})$ from the particle filter):

- Draw $(\hat{r}_K, \hat{\mathbf{x}}_K) \sim \hat{p}(r_K, \mathbf{x}_K | y_{1:K})$, i.e. select $(\hat{r}_K, \hat{\mathbf{x}}_K) = (r_K^{(i)}, \mathbf{x}_K^{(i)})$ with probability w_K^i .
- Repeat for $k = K - 1, \dots, 1$:
 - For all $i = 1$: calculate $w_{k|k+1}^i$ according eq. 16.
 - Select $(\hat{r}_k, \hat{\mathbf{x}}_k) = (r_k^{(i)}, \mathbf{x}_k^{(i)})$ with prob $w_{k|k+1}^i$.

This algorithm produces an approximation $(\hat{r}_{1:K}, \hat{\mathbf{x}}_{1:K})$ of the most likely sequence, i.e. the sequence $(r_{1:K}, \mathbf{x}_{1:K})$ that maximizes $p(r_{1:K}, \mathbf{x}_{1:K} | y_{1:K})$.

6 EXPERIMENT

We conduct experiments to evaluate the proposed

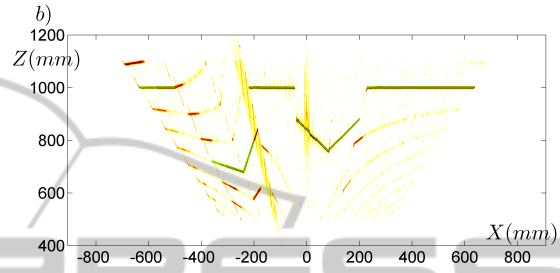
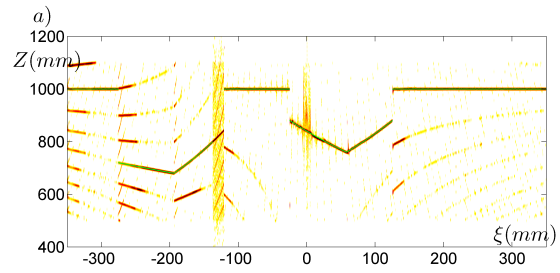


Figure 5: Estimated depths.

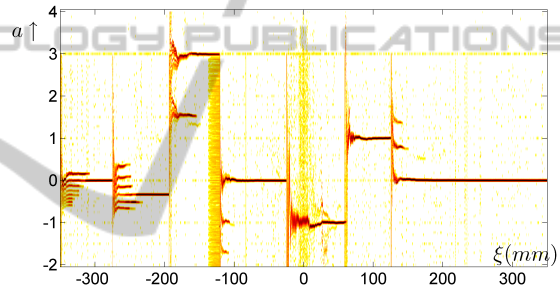


Figure 6: Estimated slopes.

algorithm. Preliminary results are presented here. The goal is to validate the algorithm. For that purpose, the system is simulated with two test scenes. The geometry of the first test scene is shown in figure 2. Parameters are as follows: camera: $D_C = 550$, $\Delta\xi = 0.5$, $K = 1400$, $B = 1$; projector: $D_P = 900$, $\Delta\eta = 0.6$, $A = 1$, $T = 20\Delta\eta$, $\sigma_v = 0.02$. The algorithm runs with $N = 200$ particles.

Figure 5 shows the resulting density estimate in the Z, ξ domain, and in the X, Z domain. After each transition, the particle filter produces a multimodal distribution, but after a few steps, the curved solutions die out. Within each continuity interval, the only survival is the true linear segment. Figure 6 shows the resulting density of the slopes a_k of these segments. Within each continuity interval, the slope is first multimodal, but after some steps it becomes unimodal. Figure 7 shows the number of samples of each mode for the first 120 steps. Most modes die out after 50 steps. These modes are the one that are most curved. Two modes, however, are only slightly curved and die after about 100 steps.

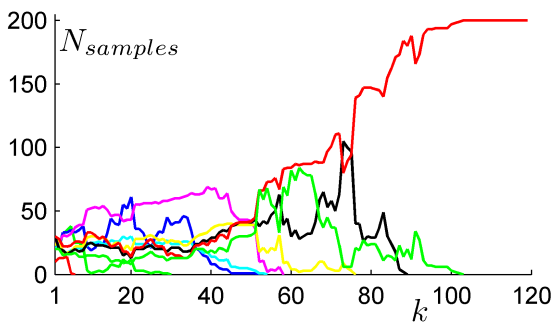


Figure 7: Nr. of samples/mode.

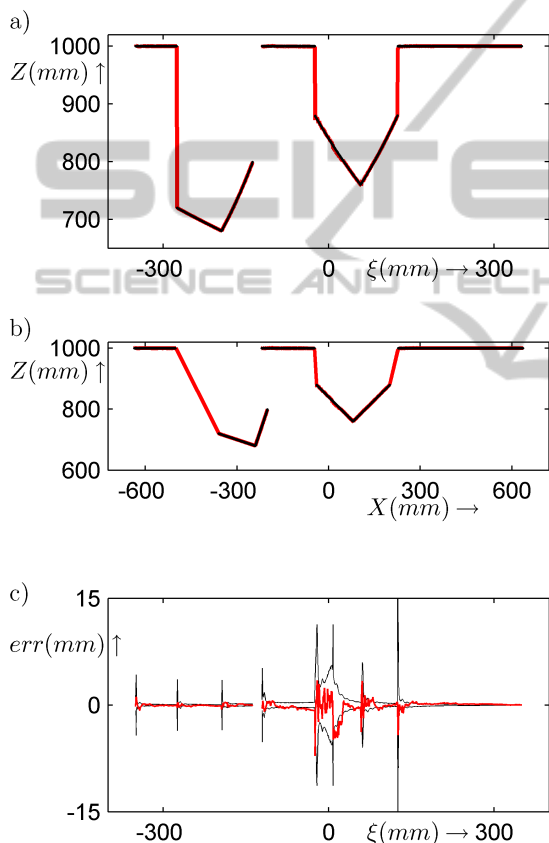


Figure 8: Results after particle smoothing. a) and b) Smoothed estimates in the Z, ξ and the Z, X domain. Red thick line = estimate; black thin lines = ground truth. c) Estimation errors and indicated standard deviations.

We also observe in figure 5 and 6 that the linear segments are found faster if they are more in the vicinity of the optical axis of the projector. This is due to the fact that the ambiguous trajectories are more curved near the optical axis, as shown in figure 4. At the optical axis, the measurement does not provide any information about the depth. Yet, our model driven particle filter provides an estimate there, though at the cost of a larger noise sensitivity.

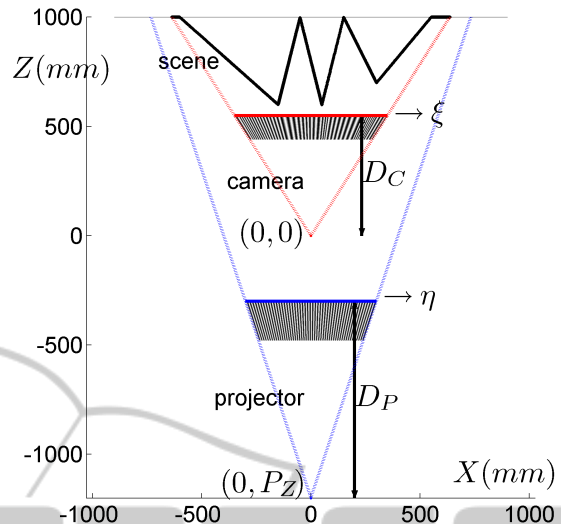


Figure 9: Test scene with walls that are near coplanar to the viewing direction.

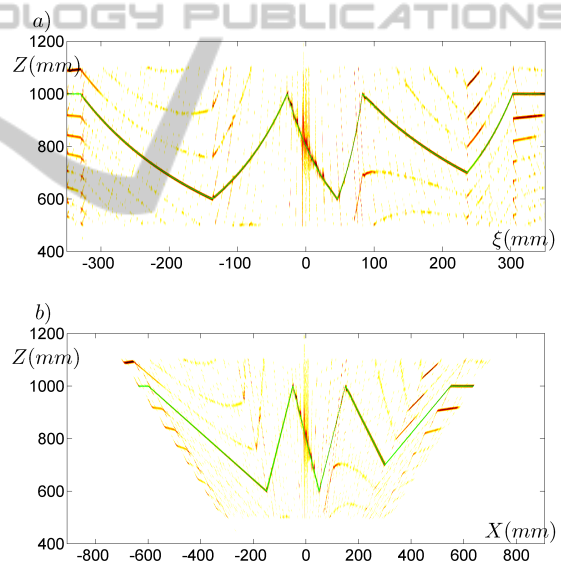


Figure 10: Particle filter depth estimates of the scene shown in Figure 9.

The results after particle smoothing are presented in Figure 8. The agreement between estimates and ground truth is quite good. The ambiguities are resolved without errors. The profile exhibits 4 step edges and 2 roof edges. All edges are detected correctly. There are no spurious edges. There is only one localization error, which occurs at the roof edge near $\xi = 60$. The cause can be traced back to the particle filter. The roof edge has discontinuities in the derivatives, but the profile itself is continuous. Thus, the measurements are only slowly running out of line

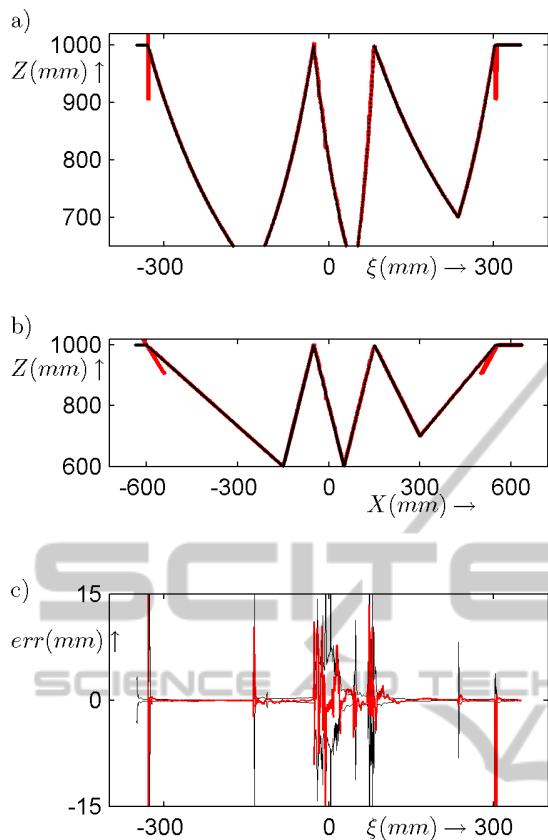


Figure 11: Results after smoothing.

with the currently estimated mode. Once a delay in localization occurs, it cannot be undone by the backward smoother because the smoother doesn't rely on measurements. The accuracy of the depth estimates is depicted in Figure 8c. The standard deviation, obtained from the EKF, is in line with the real estimation errors. We observe that, scanning from left to right, at each edge the standard deviation jumps to a higher level, and then decays. The explanation is that our smoother only selects particles, but it does not change particles. Thus, a Kalman state, stored in a selected particle, is not smoothed. Clearly, here some room for improvement.

The test scene in Figure 2 contains one region that is occluded. It can be observed in Figure 5 that the particle filter produces a uniform probability density in this area reflecting the fact that no information is available in this region. During the smoothing pass this region is removed from the map. This is easily accomplished since occlusions are reflected in the measurements by an absence of a sinusoidal pattern.

We also tested the algorithm to a scene with objects whose main planes are near coplanar to the viewing direction. The scene is shown in Figure 9. The imaging parameters are the same as in the first exam-

ple. The result of the particle filter and the smoother are shown in Figure 10 and 11, respectively. Although in these figures, the algorithm is successful (it finds the correct solution), multiple runs of the algorithm, with different random seeds, shows that this is not always the case. Especially, in the left part of the scene it may happen that the algorithm gets stuck in the wrong mode. A possible explanation for this behaviour might be that the number of ambiguities on the sides of the images is much larger than in the central part. Moreover, all those solutions are near linear. This is quite opposite to the central part. In fact, on the optical axis of the projector the solution is unique, and near the optical axis all spurious solutions are highly curved.

7 CONCLUSIONS

This paper demonstrates that the ambiguity problem in phase measuring profilometry can be solved if the solution space is limited to polyhedral objects, and if the geometrical set-up is suitably chosen. For that purpose we have developed a new particle filter that is inspired on jump Markov linear models. As a first step, we have validated this design with a demonstration on simulated data. Currently we are conducting additional experimentation on real data for a more comprehensive evaluation with respect to accuracy and reproducibility.

REFERENCES

- Arulampalam, M. S., Maskell, S., Gordon, N., and Clapp, T. (2002). A tutorial on particle filters for online nonlinear/non-gaussian bayesian tracking. 50(2):174–188.
- Doucet, A., Gordon, N. J., and Krishnamurthy, V. (2001). Particle filters for state estimation of jump markov linear systems. 49(3):613–624.
- Fong, W., Godsill, S. J., Doucet, A., and West, M. (2002). Monte carlo smoothing with application to audio signal enhancement. 50(2):438–449.
- Su, X. and Chen, W. (2001). Fourier transform profilometry: A review. *Optics and Lasers in Engineering*, 35(5):263–284.
- van der Heijden, F., Spreeuwens, L. J., and Nijmeijer, A. C. (2009). One-shot 3d surface reconstruction from instantaneous frequencies - solutions to ambiguity problems. In *Int. Conf. on Computer Vision Theory and Applications VISAPP2009*, Lissabon. Visigrapp.